PLOS COMPLEX SYSTEMS

RESEARCH ARTICLE

Long-range temporal correlation development in resting-state fMRI signal in preterm infants: Scanned shortly after birth and at term-equivalent age

Johann P. Drayne[1], Allison E. Mella[2], Mia M. McLean[3], Steven Ufkes[4], Vann Chau[5], Ting Guo[5], Helen M. Branson[6], Edmond Kelly[7], Steven P. Miller[3,5], Ruth E. Grunau[3], Alexander M. Weber[3]*

1 Department of Physics & Astronomy, The University of British Columbia, Vancouver, BC, Canada, **2** Department of Neuroscience, The University of British Columbia, Vancouver, BC, Canada, **3** Department of Pediatrics, The University of British Columbia and BC Children's Hospital Research Institute, Vancouver, BC, Canada, **4** Centre for Computational Medicine, The Hospital for Sick Children and University of Toronto, Toronto, ON, Canada, **5** Department of Pediatrics, The Hospital for Sick Children and University of Toronto, Toronto, ON, Canada, **6** Department of Medical Imaging, The Hospital for Sick Children and University of Toronto, Toronto, ON, Canada, **7** Department of Pediatrics, Mount Sinai Hospital and University of Toronto, Toronto, ON, Canada

* aweber@bcchr.ca

Abstract

While the newborn's brain is functionally organised early on—with similar resting state networks as those of adults present at birth—these networks continue to develop at different rates and in complex ways over time. While most *in vivo* functional imaging studies examine the spatial characteristics of resting state networks (RSNs), such as their size or the degree of connectivity, the temporal characteristics of these networks are less well characterised. We set out to examine the long-range temporal correlation (LRTC) of the fMRI blood oxygen level-dependent (BOLD) signal using the Hurst exponent in various RSNs in infants born very preterm shortly after birth (< 32 weeks gestational age; n = 64) and again later at term equivalent age (TEA) (n = 69). The Hurst exponent in grey matter and white matter was 0.69 at preterm age and increased significantly to 0.80 at TEA, with a greater difference between the tissues at TEA. The Hurst exponent in RSNs similarly was found to be approximately 0.68 for most networks at preterm age but increased significantly at different rates by TEA: 0.77 and 0.76 in the cerebellum and frontal networks respectively, and 0.84 and 0.83 in the motor and visual networks respectively. This pattern is partly consistent with findings from previous functional connectivity fMRI studies that the general growth and maturation of RSNs occur first and develop more quickly in sensory and motor networks, but later in associative networks like frontal ones. Importantly, this is the first time that this pattern has been shown in the LRTC of the fMRI BOLD signal itself, an area of study that may provide greater insight into functional brain development.

OPEN ACCESS

Citation: Drayne JP, Mella AE, McLean MM, Ufkes S, Chau V, Guo T, et al. (2024) Long-range temporal correlation development in resting-state fMRI signal in preterm infants: Scanned shortly after birth and at term-equivalent age. PLOS Complex Syst 1(4): e0000024. https://doi.org/10.1371/journal.pcsy.0000024

Editor: Kosmas Kosmidis, Aristotle University of Thessaloniki: Aristoteleio Panepistemio Thessalonikes, GREECE

Received: April 1, 2024

Accepted: October 14, 2024

Published: December 5, 2024

Peer Review History: PLOS recognizes the benefits of transparency in the peer review process; therefore, we enable the publication of all of the content of peer review and author responses alongside final, published articles. The editorial history of this article is available here: https://doi.org/10.1371/journal.pcsy.0000024

Data Availability Statement: All code and pipelines used to process the MRI data are available on our

github repository under the code folder: https://github.com/WeberLab/LRTC_PLOSComplex/tree/main/code All statistical analysis code performed after MRI processing are available on the same github repository under the stats folder: https://github.com/WeberLab/LRTC_PLOSComplex/tree/main/stats Raw MRI images data can not be made publicly available under the SickKids Research Ethics Board (REB). In order to comply with the research ethics board restrictions, we are unable to make the MRI scans publicly available due to privacy concerns. We can, however, consider reasonable requests from investigators with whom we are able to develop appropriate data transfer agreements and obtain research subject consent. For further inquiries, please contact the Sickkids REB at ask.crs@sickkids.ca.

Funding: This study was supported by an establishment award (AMW), and investigator salary awards (AMW, REG) from the British Columbia Children's Hospital Research Institute. Canadian Institutes of Health Research (CIHR MOP-136966), CP Alliance (PG-016817), Ontario Brain Institute and Brain Canada (The Canadian Neonatal Brain Platform). MAM was supported by a CIHR Postdoctoral Fellowship Award, and Michael Smith Foundation for Health Research Trainee Award. The funders had no role in study design, data collection and analysis, decision to publish, or preparation of the manuscript.

Competing interests: The authors have declared that no competing interests exist.

Author summary

In our study, we explored how the brains of babies born earlier than normal develop up until the time when most babies are born. We used a special technique that examines the complexity of the functional activity of different regions of the brain. What we discovered was that starting shortly after birth, the measure of complexity was more random than ordered. However, as the babies got older, all areas of their brain showed functional activity that became more ordered. Moreover, it appears that some areas of the brain, such as those responsible for moving and seeing, became more ordered faster than other areas, such as ones located in the frontal area of the brain. This insight into how brains develop in the early weeks of life, from more random to more ordered, and in some regions more than others, may help inform neuroscientists and clinicians about what is happening to the brain in the earliest stages of life outside the womb.

Introduction

Being born very preterm (< 32 weeks gestational age [GA]) is associated with altered brain maturation [1, 2], which contributes to neurodevelopmental and behavioural problems into adulthood [3–7]. These include increased susceptibility to major impairments such as cerebral palsy, or to learning disabilities, attention problems, and more internalising (anxiety and depressive) symptoms [8]. These are likely due, at least in part, to the disruption of critical aspects of brain development, including dysmaturation of myelination and synaptogenesis [9], as well as critical brain networks [10]. Identifying the alterations that occurs with preterm birth and how altered brain processes progress to term equivalent age (TEA) could aid in the understanding of how the brain develops during the third trimester of gestation outside the intrauterine environment.

More conventional MRI methods of structural, diffusional, and functional techniques have all been utilised to explore disruptions in the preterm brain in comparison to term born controls. Resting state fMRI (rs-fMRI) is of particular interest in infants due to the ability to assess brain function in the absence of a task. Resting state networks (RSNs) have been found in infants born preterm as early as 26 weeks postmenstrual age similar to those of adults [11, 12]. Most rs-fMRI studies, however, have focused on the spatial connectivity of these networks. An alternative fMRI analysis technique that examines the power-law and scale-invariant behaviour of time-series, however, can be used to analyse the temporal dynamics of the fMRI signal and measure its complexity. Theories have been put forward that the brain evolved to exist in a complex/critical state between order and disorder in order to maximise efficiency, storage capacity, and flexibility [13]. Clinically significant changes in fMRI signal complexity, as measured using the Hurst exponent (HE), have been found in Alzheimer's disease [14], schizophrenia [15], autism spectrum disorder [16, 17], acute intoxication [18], mild traumatic brain injury [19], and more [20]. In studies of adults, the HE of grey matter at rest is usually found to be between 0.7 and 1, and is known to decrease when performing a task [21, 22]. This decrease in HE is believed to be due to a need for distributed network performance (i.e. slow precision over fast decision processing) [23]. The HE has also been demonstrated to have excellent test-retest reliability [21, 24–26]. To our knowledge, this technique has not yet been in investigated longitudinally in preterm newborns using low-sampled fMRI ($\sim$ 100 volumes).

Previous studies have explored brain oscillations and complexity in groups of infants, school-age children and adults. A study conducted by Padilla et al. (2020) analysed neural

activity and brain criticality in a group of 10-year-olds who were born extremely premature compared to term born children [27]. Using a novel fMRI 'intrinsic ignition' analysis, they found that the extremely premature group demonstrated suboptimal synchronicity and criticality to controls [27]. Through the use of electroencephalography (EEG), Hartley et al. (2012) analysed burst activity with the HE in a group of 11 preterm infants born between 23 and 30 weeks of gestation and discovered LRTC that indicated phase transition [28]. However, their discovery regarding patterns of complex organisation in the preterm brain was done with EEGs recorded only once shortly after birth without follow up at term-equivalent age [28]. It is crucial to understand how signal production and complexity evolves in different brain networks from the premature early life to TEA. In this study, we set out to investigate the HE of the blood oxygen level-dependent (BOLD) signal of rs-fMRI to determine changes in brain signalling complexity from shortly after birth to TEA in various resting-state brain networks in very preterm infants. This approach can therefore inform us about how the temporal dynamics of different brain networks mature from more random to more ordered states.

Materials and methods

Participants

Very preterm infants (< 32 weeks GA) admitted to the neonatal intensive care units (NICUs) at the Hospital for Sick Children and Mount Sinai Hospital, Canada were enrolled. Research Ethics Boards at both hospitals approved the study following the guidelines of the Declaration of Helsinki. Inclusion criteria: preterm born infants (both singleton and multiple gestation preterm infants) less than 32 weeks' gestation receiving standard clinical care in the NICU at each study site (SickKids, Mount Sinai Hospital). Exclusion criteria: clinical evidence of a congenital malformation or syndrome; congenital TORCH infection; international patients and those residing outside of Ontario; and short stays (less than 3 days). Written informed consent was obtained from parents/legal caregivers. Neonatal research nurses collected demographic data and clinical variables systematically.

Magnetic resonance imaging

Infants were scanned without sedation in an incubator (Lammers Medical Technology, Luebeck, Germany) on the same Siemens (Erlangen, Germany) 3T Tim Trio MRI scanner and single-channel neonatal head coil (Advanced Imaging Research, Cleveland, OH) at the Hospital for Sick Children, Toronto. MRI scans were acquired at preterm age shortly after birth (median postmenstrual age [PMA] of 32.6 weeks, range: 27.3 to 37.9), and later at TEA (median PMA of 40.7 weeks, range: 34.7 to 48.1).

Anatomical images were acquired using a T1-weighted sequence (repetition time [TR], 6 ms; echo time [TE], 2.64 ms; field of view [FOV], 150 x 192 × 96 mm; voxel size: 1 mm isotropic; 96 slices; slice overlap, 8.3%); and a T2-weighted sequence (TR, 5,040 ms; TE, 143 ms; FOV, 104 x 128 x 110 mm; 110 slices; voxel size, 1 mm isotropic). Resting-state fMRI was acquired using an echo-planar imaging sequence (TR, 3000 ms; TE, 50 mc; FOV, 192 x 192 x 111 mm; slice thickness, 3 mm; 37 slices, voxel size, 3 mm isotropic, 100 volumes). An EPI fieldmap was also acquired (TR, 600 ms; TE1, 5.19 ms; TE2, 7.65 ms; FOV, 252 x 252 x 100 mm; 50 slices; slice thickness, 2 mm; voxel size, 3 x 3 x 2 mm).

Data processing

The documentation and code for our analysis can be found on Github at: https://github.com/WeberLab/LRTC_PLOSComplex. Fig 1 depicts the simplified MRI analysis steps in a

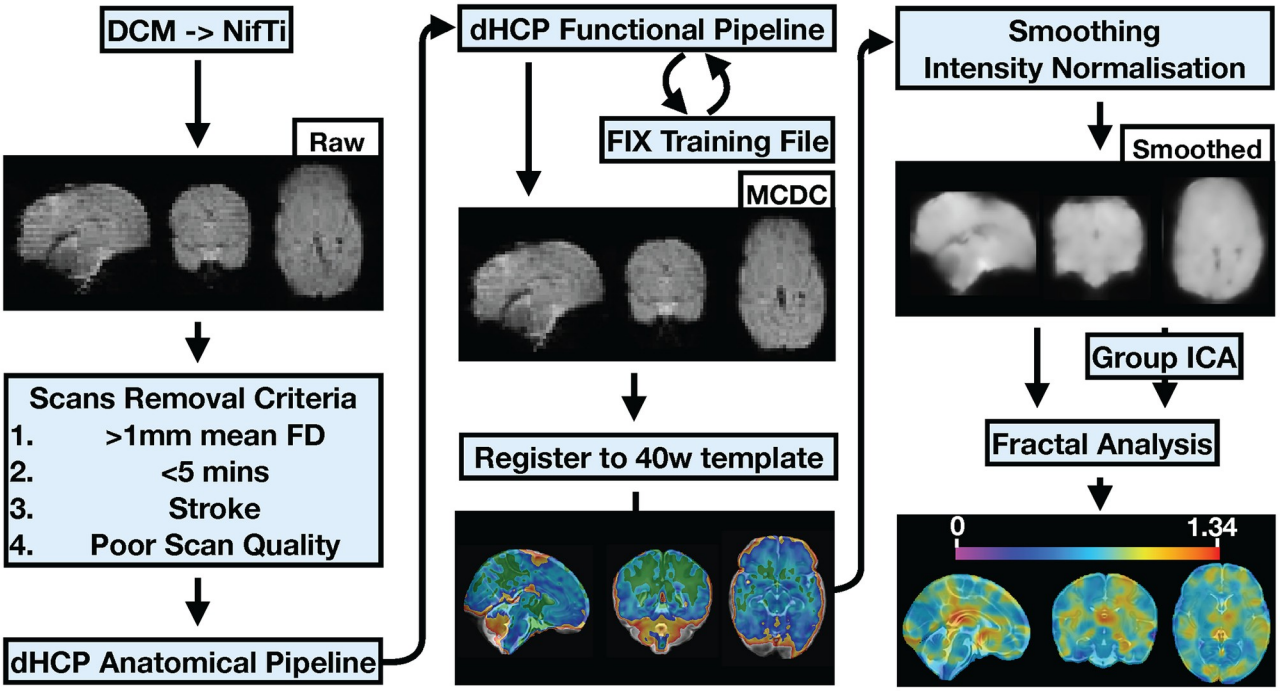

Fig 1. Work-flow of post-acquisition processing steps. Figure visualises distinct steps in the work-flow of the image processing pipeline.

https://doi.org/10.1371/journal.pcsy.0000024.g001

flowchart. To begin, all DICOM files of interest were converted to NIfTI format (Neuroimaging Informatics Technology Initiative) using Chris Rorden's `dcm2niix` [29].

Anatomical analysis. Anatomical images (T1w and T2w) were manually inspected for quality control or, if there were multiple scans, to find the scan with the best quality by both J. D and A.M.W. Images with very poor tissue contrast or motion artefacts were rejected. Next, T1w and T2w images were bias-field corrected using ANTs N4ITK [30]. For each subject, the T1w image was rigidly registered to the corresponding T2w image using ANTs registration [31]. The images were then skull-stripped and segmented using the dHCP anatomical pipeline [32]. The dHCP pipeline first uses FSL's `bet` [33] to perform an initial skull-stripping with a fractional intensity threshold of 0.1. Tissue segmentation is then accomplished using the DRAW-EM algorithm [34], which uses an atlas-based segmentation technique and an Expectation-Maximization scheme that combines the structure priors and an intensity model of the volume. Grey matter, white matter, and ventricle binary masks were used for subsequent HE analysis.

Resting state fMRI analysis. fMRI scans with less than 98 time-points (length of 4 mins 54 sec) were removed completely from the study. To reduce the contribution of motion artefacts, FSL's `MCFLIRT` [35] was performed on all fMRI datasets to determine the amount of head motion during the scan and align volumes. To determine average motion, mean frame-wise displacement (meanFD) was calculated as the average of the sum of the absolute values of the differentiated realignment estimates (by backwards differences) at every time point [36]. Rotational displacements were first converted to translational displacements by projection to the surface of a 50 mm radius sphere. Scans with a meanFD > 1 mm were excluded. Volume censoring was not practical as fractal analysis requires many sequential timepoints, with 100 timepoints already on the low end of the desired number of volumes [14, 20]; see Limitations for more discussion.

Fieldmaps were generated using a dual-echo EPI and magnitude scan. The dHCP functional pipeline [37] was then implemented to achieve distortion-correction and motion-correction, register the functional image to the corresponding T2w structural image, generate a transform matrix from functional space to the 40-week T2w template, and perform temporal high-pass filtering (150 s high-pass cutoff) and independent component analysis (ICA) denoising using ICA FIX [38, 39].

ICA Fix. 26 scans were randomly selected (13 preterm and 13 TEA) to run through the dHCP functional pipeline until the FIX stage. ICA components were manually classified [40] using an "innocent until proven guilty" strategy as suggested by Kelly et. al (2010) [41]. The training file was created using FSL's `FIX` [38, 39]. The dHCP functional pipeline was then run on all subjects using the study-specific training file. The standard space was set at a 40-week-old template from the dHCP pipeline. Spatial smoothing of 5 mm was applied using FSL's `SUSAN` [42] and grand mean intensity normalisation was computed.

Group RSN maps. Using FSL's `MELODIC` [43], group ICA was performed with 20 dimensions on all subjects in the 40-week template space to obtain shared RSN maps. While it is true that RSNs change over time from preterm age to TEA, these changes are not very drastic [44]. In order to compare changes in HE in the same networks over time, we chose to run the group ICA across all ages together. All 20 RSNs were manually inspected independently by J.D. and A.M.W. Nine networks were identified that were deemed similar to previously published networks in preterms [44]. RSNs were then thresholded (set to zero) below 5 standard deviations and binarized to create network masks; see Fig 2.

Hurst exponent calculation. fMRI signal LRTC was examined using the HE. HE can be calculated from the slope of the log-log plot of the power spectral density (PSD), which describes how the power of the fMRI signal (here taken as the square of the absolute frequency) is distributed over the frequency. If beta is the slope, then HE is calculated as Eq (1).

$$\mathrm{HE} = \frac{1+\beta}{2}, \tag{1}$$

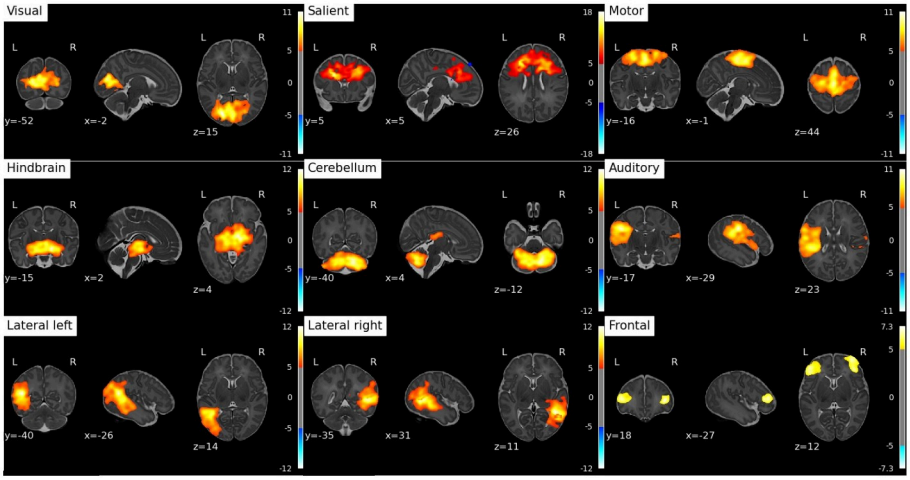

Fig 2. Group resting state networks. Spontaneous activity patterns shared between preterm and term equivalent age of infants born prematurely. Example sagittal, coronal, and axial slices for meaningful spatial patterns (corresponding to independent components from probabilistic ICA) are overlaid onto the 40 week age template. Overlay images are z-statistic maps thresholded at 5. From left-to-right and top-to-bottom: Visual, Salient, Motor, Hindbrain, Cerebellum, Auditory, Lateral Left, Lateral Right, and Frontal.

https://doi.org/10.1371/journal.pcsy.0000024.g002

The β value can help determine a signal's class, where $\beta < 1$ is usually fractional Gaussian noise (fGn) and $\beta > 1$ is usually fractional Brownian motion (fBm) [45]. fGn signals are stationary processes with constant variance, whereas fBm signals are non-stationary processes with increasing variance over time. Bullmore et al. (2004) have shown that most of the brain fMRI signals that are initially characterized as fBm will become fGn with proper motion correction [46]. As this will not completely remove all fBm signals, we have made use of the "extended HE" (HE′), first conceptualised by Eke et al. (2000) [45], where $0 < \mathrm{HE}' < 1$ describes fGn processes and $1 < \mathrm{HE}' < 2$ describes fBm processes. HE′ values will be used in this analysis, but from this point forward shall be referred to as HE.

The PSD was calculated using Welch's method [47], using the `welch` command from Python's `Scipy.Signal` library [48], with eight windows of 50% overlap on a restricted frequency range of the data (above 0.01 Hz), mirroring the parameters used by Rubin et al. (2013) [49]. Welch's method was chosen because it has been found to outperform alternative methods (such as wavelet or rescaled range analysis) [49]. The mean HE was then calculated for all ROI masks: grey matter, white matter, and all nine RSNs for each subject.

Statistical analysis

All statistical analyses were performed in R [50] and RStudio [51]. Because some subjects had repeat scans (preterm and TEA) while others had only one (either preterm or TEA), a linear mixed effects model (LMEM; `lme4` [52]) analysis was used with subjects as random effects. To determine if GA was a factor in missing values at TEA, we performed a student's unpaired t-test between infants scanned at both preterm age and TEA later on and those scanned only at preterm age without TEA scans (either due to MRI data quality or availability) for GA, meanFD, and PMA. GA was found to be different between the two groups and was included in all LMEMs (see S1 Fig). HE vs PMA was explored, with GA and meanFD confounds included as fixed effects (Eq (2)).

$$\mathrm{HE}_{ROI} = \mathrm{PMA} * \mathrm{ROI} + \mathrm{GA} + \mathrm{meanFD} + (1|\mathrm{Subject}), \tag{2}$$

To determine if a fixed effect (PMA, GA, or meanFD) was a significant component of the model, an ANOVA was performed between the full model and a model without the component of interest (null model).

Estimated marginal means and trends analyses were performed with the `emmeans` package [53] to determine the means and slopes of HE vs PMA while controlling for GA and meanFD.

Results

Participant demographics

Of the initial 164 scans from 120 unique subjects, after quality control, there remained 133 scans from 98 unique subjects (81% retention of scans; 82% retention of subjects). Of the 98 subjects, there were: 28 with preterm only scans, 35 with both preterm and TEA scans, and 34 with TEA only scans. Thus, there were 63 scans at preterm age and 69 scans at TEA. More information on participant demographics can be found in Table 1.

Hurst exponent

A sample Welch's PSD averaged over the grey matter can be seen in Fig 3. The negative slope of the PSD displays the power-law behaviour that has been reported in human brain fMRI previously [22, 54–57]. Due to the long TR (3 s) and low number of volumes (100), no frequency range was specified; instead, the entire spectrum was used to calculate HE.

Table 1. Demographic characteristics of the study population.

Groups	n	Sex (M/F)	Median GA (range)	Median PMA at scan (range)
Unique subjects	98	51/47	27.4 (22.7 to 31.6)	n/a
Scanned at preterm age	63	32/31	27.7 (22.7 to 31.6)	32.7 (27.3 to 37.9)
Scanned at TEA	69	36/33	26.3 (22.7 to 31.6)	40.9 (34.7 to 48.1)

All ages in weeks. GA = gestational age, PMA = post menstrual age, TEA = term-equivalent age.

https://doi.org/10.1371/journal.pcsy.0000024.t001

Hurst exponent across tissue type and age. Mean HE was calculated within cortical grey matter, white matter, and ventricles for each subject at each age. HE in the ventricles were acquired as a surrogate of a 'noise ground floor' to compare with GM, WM and RSNs. Estimated marginal means (controlling for GA and meanFD) at 32.7 weeks PMA and 40.9 weeks PMA were calculated and compared. At preterm age (32.7 weeks), cortical grey matter HE was 0.68 (CI = 0.66 to 0.70), white matter HE was 0.67 (CI = 0.65 to 0.69), and ventricle HE was 0.66 (CI = 0.66 to 0.70). At TEA (40.9 weeks), grey matter HE increased to 0.80 (CI = 0.78 to 0.82), white matter HE to 0.78 (CI = 0.76 to 0.80 and ventricle HE to 0.78 (CI = 0.76 to 0.80). Marginal trends (controlling for GA and meanFD) were calculated and compared (Fig 4). Grey matter HE increased 0.0150 per PMA week ($p < 0.0001$), while white matter HE increased 0.0130 per PMA week ($p < 0.0001$) and ventricle HE increased 0.0136 per PMA week ($p < 0.0001$). These trends were not significantly different from each other. Looking at scans separately (preterm and TEA) and performing a paired student's t-test between the grey matter and white matter revealed significant differences at both preterm age (mean difference HE = 0.0060; effect size = 0.40 (small); $p = 0.0022$) and TEA (mean difference HE = 0.019; effect size = 1.22 (large); $p < 0.0001$) with grey matter being higher.

Hurst exponent across group resting state networks and age. Mean HE was calculated for all nine RSNs for each subject at each timepoint (Fig 5). Estimated marginal means (controlling for GA and meanFD) at 32.7 weeks PMA and 40.9 weeks PMA were calculated and

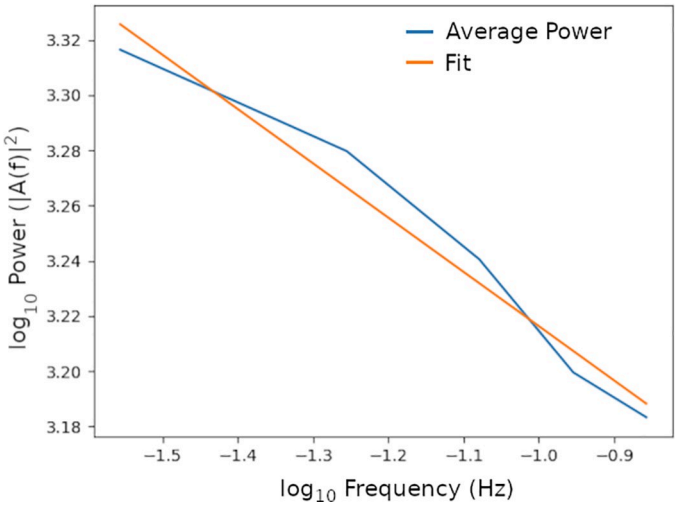

Fig 3. Sample welch's power spectral density and hurst exponent calculation. A representative sample log-log plot of the Welch's power spectral density averaged over the grey matter of one subject (blue line). The orange represents the best fit of a linear regression which is used to calculate the slope (β). The Hurst Exponent is then calculated from the slope (see Eq (1)).

https://doi.org/10.1371/journal.pcsy.0000024.g003

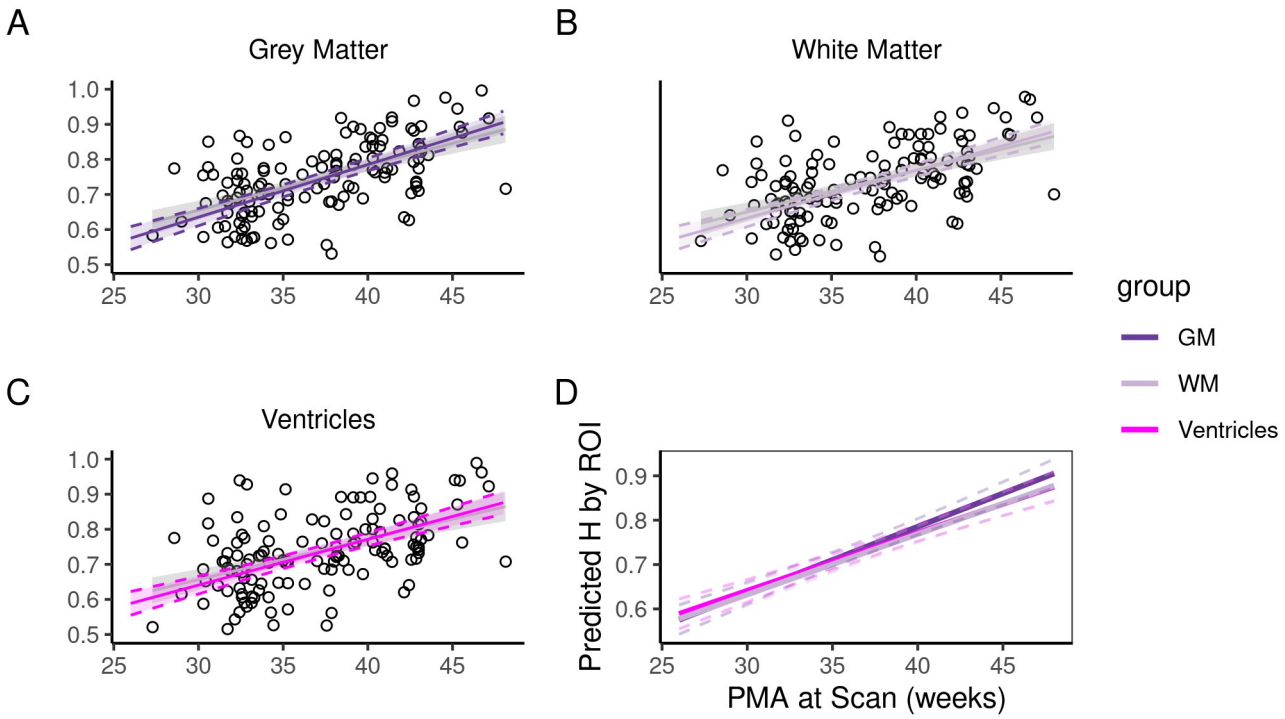

Fig 4. Hurst exponent values in grey matter, white matter, and ventricles versus postmenstrual age at scan (weeks). The effect plots in A, B and C show the marginal effects of the linear mixed effects regression model (line) and 95% confidence intervals (dashed lines) in the grey matter, white matter, and ventricles, respectively. For each of the three regions of interest [grey matter: dark purple plot; white matter: light purple plot; ventricles: magenta] we show the model-based effect on the Hurst exponent. Additionally, we show the bivariate unadjusted correlation (points, regression line, and CI in light grey in the background). In plot D, we plot the model-based effect on the Hurst exponent for both grey matter, white matter, and ventricles with 95% confidence intervals together for comparison purposes.

https://doi.org/10.1371/journal.pcsy.0000024.g004

compared—both across age within RSN and across RSN within age. At 32.7 weeks PMA, HE in all RSNs was approximately 0.67 (range = 0.66 to 0.68). At this age, the HE in these networks were not different from each other ($p > 0.05$ after adjusting for multiple comparisons). At 40.9 weeks PMA, HE increased in all RSNs to around 0.79 (range = 0.76 to 0.84). See Table 2. At TEA, HE in RSNs were different between auditory and cerebellum, auditory and frontal, auditory and salient, cerebellum and motor, frontal and motor, frontal and visual, hindrain and motor, hindbrain and visual, laterel left and motor, lateral left and visual, lateral right and motor, motor and salient, and slient and visual. ($p < 0.05$ after adjusting for multiple comparisons).

Estimated marginal means of linear trends (controlling for GA and mean FD) were calculated (Fig 6) and compared (Fig 7). Increasing HE with PMA were found in all networks. The visual, motor, lateral right, lateral left, and posterior networks were found to have larger slopes, while the salient, frontal and hindbrain networks with smaller slopes. Significant differences in slopes were found between: motor and frontal, motor and cerebellum, salient and motor, visual and cerebellum, visual and frontal, visual and hindbrain, and visual and salient ($p < 0.05$ after adjusting for multiple comparisons).

Discussion

To the best of our knowledge, this is the first rs-fMRI study that has investigated the HE of low-sampled (100 volumes) fMRI BOLD signal in preterm infants at both preterm age and

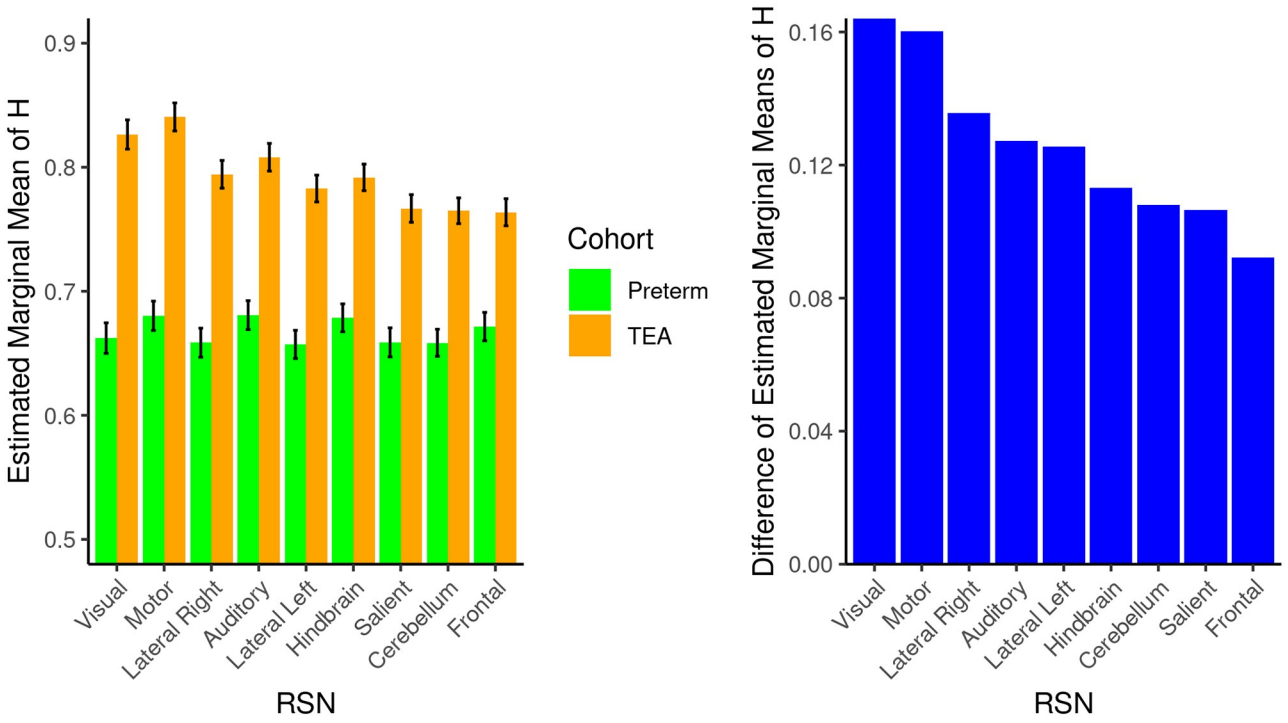

Fig 5. Estimated marginal means of the Hurst exponent. The barplot on the left displays the estimated marginal means of the Hurst exponent in each resting state network between preterm and term equivalent ages. Standard errors are displayed as error bars. The barplot on the right is the difference between preterm and term equivalent age Hurst exponents from the barplot on the left. Networks are ordered from highest to lowest difference in Hurst exponent between preterm and term equivalent age.

https://doi.org/10.1371/journal.pcsy.0000024.g005

later at TEA across multiple RSNs. We describe here the evolution of HE over time as the preterm brain develops over the period of neonatal intensive care. The two main new findings from this study are that HE in grey matter and white matter increase significantly from preterm age to term age, with a greater difference between the tissues at TEA; and HE in RSNs similarly increase significantly from preterm to term age but at different rates, with the lowest in the frontal and the highest in the visual network.

Table 2. Demographic characteristics of the study population.

RSN	HE emmeans at 32.7 weeks PMA	HE emmeans at 40.9 weeks PMA	p-value
Motor	0.680	0.841	< 0.0001
Visual	0.662	0.826	< 0.0001
Auditory	0.681	0.808	< 0.0001
Lateral Right	0.659	0.794	< 0.0001
Hindbrain	0.679	0.792	< 0.0001
Lateral Left	0.657	0.783	< 0.0001
Salient	0.659	0.767	< 0.0001
Cerebellum	0.658	0.765	< 0.0001
Frontal	0.672	0.764	< 0.0001

RSN = resting state network; HE = Hurst exponent; emmeans = estimated marginal means; PMA = post menstrual age; Plus and minus values refer to 95% confidence interval.

https://doi.org/10.1371/journal.pcsy.0000024.t002

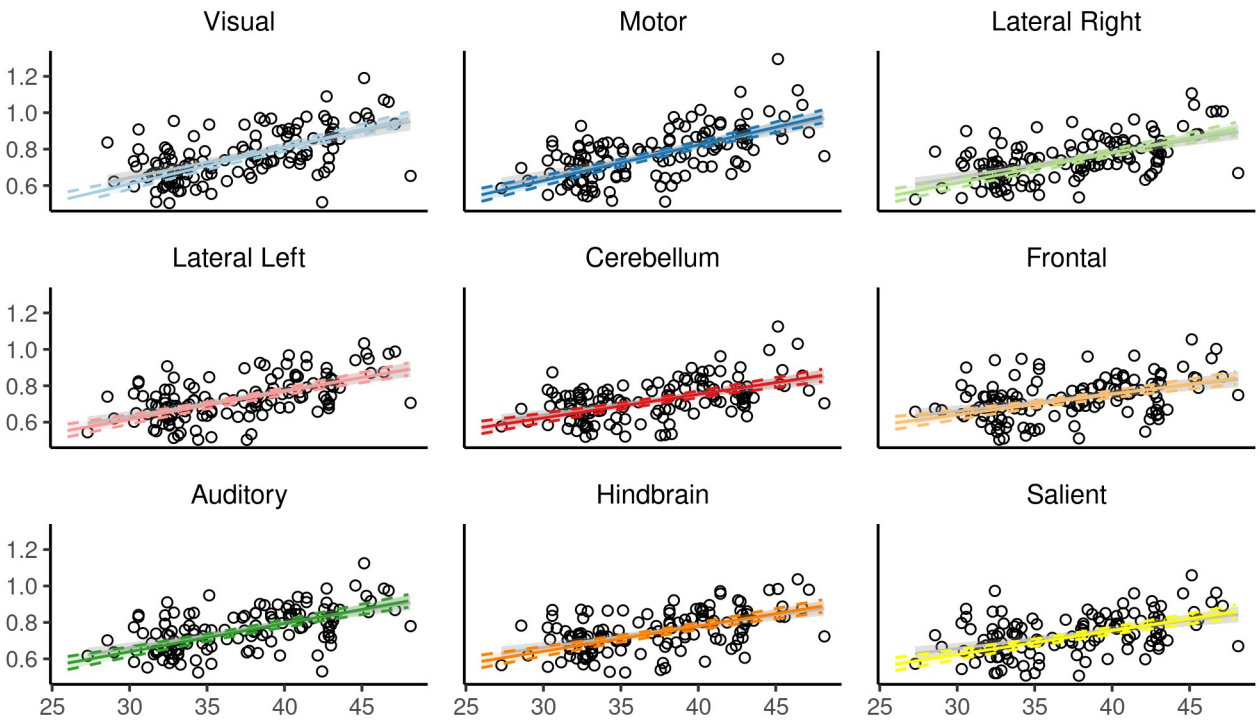

Fig 6. Hurst exponent values in group resting-state networks versus post menstrual age at scan (weeks). The effect plots show the marginal effects of the linear mixed-effects regression model (line) and confidence interval (dashed lines) in the eight shared resting-state networks. For each network we show the model-based effect on the Hurst exponent. Additionally, we show the bivariate unadjusted correlation (points, regression line, and CI in light grey in the background).

https://doi.org/10.1371/journal.pcsy.0000024.g006

What does HE measure in the brain?

While a full summary of HE and brain criticality is outside the scope of this paper, readers are directed to reviews by Campbell and Weber (2022) on HE of fMRI in the brain [20], and Zimmern (2020) for a more theoretical discussion about brain criticality [13]. In brief, HE between 0.5 and 1, which is generally found in human brain fMRI BOLD signals, indicate long-term positive autocorrelation, meaning that a high value in the series will probably be followed by another high value. Thus a signal with a HE closer to 1 is more ordered and predictable than a signal closer to 0.5. Ultimately HE is measuring the LRTC of the fMRI signal and its complexity. Complexity exists along the boundary of order and disorder [58]. This complexity has been observed at almost every level of the brain in both spatial and temporal domains: dendritic branching structures in the spatial domain [59], to neurotransmitter release [60], neuronal firing rates [61], local field potentials [62], MEG signals [63], and EEG signals [54], not to mention fMRI [63, 64]. Complexity in the brain appears to be the rule, not the exception. Why the brain would evolve this behaviour may be due to the theory that neural networks that exist in a critical state between ordered and disordered exhibit optimal processing and computing properties [65, 66]. These properties include information transmission, information storage, dynamic range, metastable states, and computational power [13, 67–72].

HE in brain tissue

In both grey matter and white matter, HE increased linearly from preterm to TEA (0.0150 per week and 0.0130 per week, respectively). Thus, as the preterm infants grew older, the LRTC of

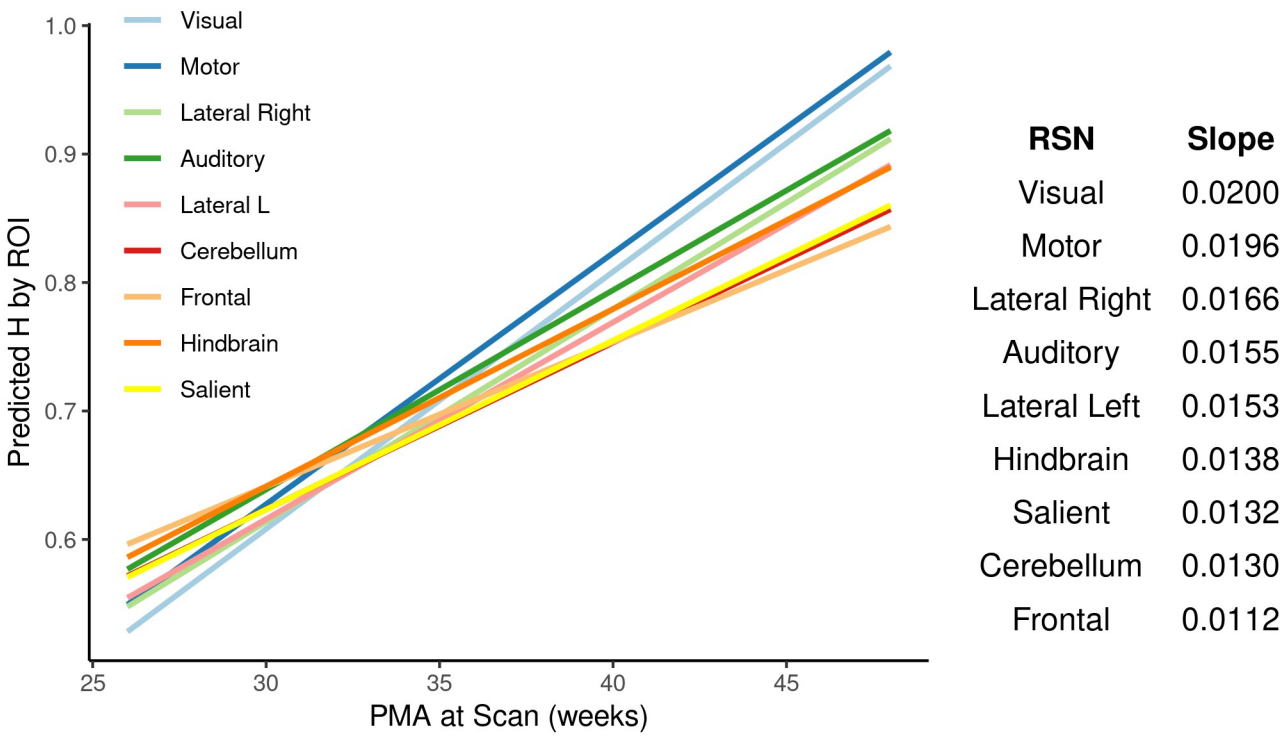

Fig 7. Comparison of Hurst exponent versus post menstrual age at scan trends across resting-state networks. Left: we plot the marginal trends from Fig 4 across all eight resting-state networks for comparison purposes. Right: a table of the slopes in descending order for each RSN is provided up to four decimal places. Significant differences in slopes were found between: visual and hindbrain, visual and frontal, visual and salient, motor and hindbrain, and lateral right and hindbrain ($p < 0.05$ after adjusting for multiple comparisons).

https://doi.org/10.1371/journal.pcsy.0000024.g007

measured fMRI signal increased, meaning these signals became more ordered with long-term memory. HE in grey matter was found to be consistently higher than white matter in infants at both preterm and TEA. This difference, however, was more pronounced at TEA, as demonstrated by the larger effect size at TEA (1.26) vs preterm age (0.73). Thus, from $\sim$32.7 weeks to $\sim$40.9 weeks, HE increases faster in grey matter than in white matter. While higher HE in grey matter could perhaps represent more ordered complexity in neuronal signalling (by way of the BOLD signal), it is less clear what HE in white matter represents. fMRI signals in white matter have historically been ignored and regressed out of the signal. While understanding what the BOLD signal in white matter represents is outside the scope of this paper, a review of this topic can be found by Grajauskas et al. (2018) [73].

Perhaps a more surprising finding is the increase of HE in the ventricles, a region without neuronal tissue. Previous studies that investigated the BOLD signal in ventricles using high resolution fMRI at 7T reported that these regions will overlap with larger pial and ependymal veins near ventricular cerebrospinal fluid [74], especially with lower resolution fMRI. Thus, fMRI/T_2^* signals in the ventricles may be related to neural activity by way of blood volume changes, but not differences in blood oxygenation. In turn, increases in HE in the ventricles may represent an increase in ordered complexity of the brain as a whole. However, an alternative explanation may lie in a confounding variable that we cannot rule out in this study.

Comparisons to other studies

Signal complexity in fMRI of white matter and grey matter in healthy ageing adults has been previously investigated by Liu et al. (2013) using approximate entropy (ApEn) [75]. While HE

and ApEn are not the same measures, they should by definition be negatively correlated. That is, an HE closer to 1 will have greater LRTC, and thus be more predictable (lower entropy), and vice versa. This has been shown empirically by Sokunbi et al. (2014) [15]. Liu et al. (2013) reported decreased ApEn (similar to an increase in HE) in both grey and white matter between young (age 23 ± 2 years, n = 8) and old cohorts (age 66 ± 3 years, n = 8) [75]. A similar finding, this time using HE, was found by Dong et al. (2018) when looking at 19–85 year olds (n = 116) [76]. They found a positive correlation ($r = 0.35$, $p < 0.01$) of HE with age. Both of these studies are in line with our finding of increased HE from preterm to term age in both grey and white matter, suggesting that HE increases across the entire lifespan in these tissues taken as a whole.

Dong et al. (2018) also looked at different regional changes in HE across their age range [76]. Using anatomically defined brain regions, they found that with increasing age: HE increased in the frontal and parietal lobes but decreased in the insula, limbic, and temporal lobes [76]. In our study in the developing brain, it is the sensory networks (motor, visual and auditory) that displayed the greatest increase, with the frontal regions—while also increasing—showing the least amount. Thus the frontal lobe, which is one of the highest-order regions of the brain, may take the longest to fully develop, and even continue developing late in life. On the other hand, the hindbrain, which we found to be one of the slowest to develop in newborns, seems to be one of the first regions to show decreased HE with greater ageing (insula and limbic) [76].

The reduction in HE in adult ageing may be due to a gradual loss of both local and long-range connections as a consequence of cell loss, synaptic degeneration, blood flow reduction, neurochemical alteration as well as central nervous system reorganization [75]. Thus, our findings of increased HE in all tissue and RSNs may be due to the exact opposite process: as the preterm brain grows, there is a dramatic increase in local and long-range connections due to growing cells, synaptic connections, increased blood flow and myelination [77].

In terms of studies that looked at direct comparisons between newborns and adults, Fransson et al. (2013) looked at power-law behaviour in RSNs in healthy term newborns (n = 18) compared to adults (n = 17, age 22–41 years, mean 29 years) [78]. The networks that they examined were sensory, auditory, visual, default, attention, subcortical and saliency. They reported the slope of the power law distribution as the 'power-law exponent, α' as opposed to HE. However, this α value can be converted to HE using Eq (1) above. For our purposes, it is enough to know that higher 'α' values are similar to higher HE values. In the newborn cohort, they found the sensory, auditory and visual networks to have the highest α and the subcortical, attention, saliency and default to have the lowest, in line with our results [78]. In adults, they found the visual and default networks to have the highest α values, then the sensory, attention and saliency, and finally the auditory and subcortical networks to have the lowest. Similarly, Campbell et al. (2022) using the seven Yeo networks, reported the highest HE values in the visual, frontal, default and dorsal attention, followed by somatosensory and ventral attention, and finally the limbic having by far the lowest [20]. Thus, in newborns, primary sensory areas exhibit larger power-law exponents than higher associative cortical areas, in contrast with the adult brain. The changes observed by Fransson et al. (2013) from newborn to adulthood appear to be driven by a reduction in α values across the board, except in the case of the default network which appears to remain the same [78].

Why networks mature at different rates. From 27 to 31 weeks RSNs are first identified and then continue to expand with increasing age [44, 78, 79]. A study which assessed RSNs in very preterm infants all born before 27 weeks GA and scanned at TEA found the presence of RSNs of the primary visual areas, somatosensory and motor regions, temporal/inferior parietal cortices, lateral parietal cortex and the prefrontal cortex [80]. The authors later found these

networks in a cohort of healthy term born infants [81]. Another study, which investigated 31–42 week infants discovered that regions of the primary sensorimotor, visual, auditory, language areas and subcortical areas were found to have the most significant age-dependent increases in functional connectivity [79]. Although no statistically significant differences were found between preterm infants scanned at TEA to term born controls, Doria et al. (2010) found visual, auditory, somatosensory, motor, default mode, frontoparietal and executive control networks all developed at different rates in terms of their spatial topology [44].

The findings of increased HE development in visual, auditory, and sensorimotor networks by TEA in our results is consistent with behavioural observations of prematurely born infants [82]. The different maturation timelines of primary sensory and motor networks before high order networks have been theorised to be due to evolutionary survival mechanisms for adapting into the external environment required by the primary systems, to promote basic survival functions by the time of birth and for sensory processes to trigger higher cortical networks development [44, 79, 82]. This is further exemplified with Gao et al. (2015) who found that primary sensorimotor, auditory and visual networks mature before executive control networks in a longitudinal study of infants [83]. Perhaps these findings should not come as a surprise as foetal observations of voluntary movement and sensory processing in these networks are shown to have adult-like topology earlier than other high order networks [83]. On the other hand, caution should be used when interpreting these findings of neural activity from indirect measures (e.g. fMRI). In their review of spontaneous activity in the pre- and near-term infant, Colonnese and Khazipov (2012) suggest that the generative mechanism for brain activity in this period is likely different from adults: in infants, this activity is likely involved in circuit formation, while in adults it is likely due to attention [84].

The third trimester of pregnancy is critical for the growth and extensions of thalamocortical neurons throughout the frontal, somatosensory and auditory cortex [77]. Numerous developmental processes including synaptogenesis and white matter myelination influences the formation of functional connections [11]. Connectivity between the thalamus and cortex form and neuronal connectivity at the subplate occurs early on in gestation [11]. From there, endogenous processing, sensory activity and environmental stimuli impacts neuronal size, type and distribution [11]. Myelination is critical for establishing efficient information processing and thus sustaining functional connections that form during development [11]. This process begins in the human brain during the second trimester of pregnancy [85]. Postmortem studies have revealed that myelination develops earlier and faster in patterns of proximal pathways than distal, sensory pathways than motor, and in the occipital pole than posterior parietal, temporal and frontal lobes [85]. Thus, our finding that the visual functional network has the greatest increase in HE could potentially be explained by this. Indeed, Hagmann et al. (2010) used diffusion tensor imaging tractography and rsfMRI in a cohort of 2 to 18 year olds found that with age there was a positive correlation between structural and functional connectivity [86]. One issue with this myelination hypothesis, however, is that there is very little myelination between the third trimester and TEA [87]. Most myelination occurs after full term birth in an exponential explosion of growth [85, 88]. Furthermore, this theory would predict that the brainstem would have the highest HE, while in fact it has the lowest. Thus, while it is likely that myelination plays a role in determining HE, it appears to only be a part of the explanation.

Various stimuli have effects in shaping the structural and functional cortical architecture at this highly vulnerable stage of development and preterm birth has impacted on these processes as well. Future studies should aim to investigate the preterm infant population and compare the findings to term born controls, as well as acquire multimodal MRI data such as myelin water imaging to make a direct comparison.

Limitations

There are several limitations of our study that should be highlighted. LRTC analysis has many different names (e.g.: power-law, scale-free, fractal, Hurst exponent (used here)), analysis techniques (e.g. Welch's method (used here), detrended fluctuation analysis, discrete wavelet transform, rescaled range analysis), and assumptions (gaussian vs Brownian noise, mono- vs. multi-fractal, power-law vs log-normal or Poisson distribution). Although the field has existed for 20 years, the research community is still lagging in terms of finding a common language, analysis technique, and best practice (e.g. sampling rate, number of time-points, frequency range). We have used the term LRTC here as we believe it is the least controversial description. We have used Welch's method as it has been shown to perform the best when directly compared to other methods [49]. However, as our analysis was retrospective and not part of the original study plan, we believe future studies would do better to: acquire more time-points (closer to 500); and a higher sampling rate (< 1 s). We also did not acquire healthy term controls, which would have allowed us to compare how infants born preterm compared to healthy term controls at TEA, or foetal resting state analysis which would have allowed us to make comparisons at similar post-menstrual ages between preterm and in-utero brain development.

Furthermore, our method for determining RSNs using independent component analysis is inherently linear. However, given the non-linear nature of fMRI signals, non-linear models of functional connectivity, such as Convergent Cross Mapping [89] and Optimal Information Flow [90], may be a more appropriate for determining RSNs [91, 92]. Future studies, beginning with healthy adult volunteers, should investigate whether nonlinear functional network connectivity offers deeper insights into the HE of fMRI signals. Moreover, our study did not include a comprehensive uncertainty analysis, which could help identify key determinants of model/data indicator variability and universal determinants of HE. Techniques such as global sensitivity and uncertainty analsyis (GSUA) can be used for some model-based approaches [93, 94]. As the HE is a direct calculation, however, these techniques would not work. Monte Carlo simulations could potentially be used in future studies to investigate the uncertainty in the HE and identify its stability and source [95].

Future investigations

Our findings suggest there is more work that can be done in future investigations. As mentioned previously, including healthy term controls would allow one to determine if preterm networks at TEA display higher or lower HE values. For example, does being born early, and being able to have greater visual and motor inputs, allow for faster brain development in the visual and motor networks?

Or, would being born prematurely, with the elevated risk of white matter injuries and haemorrhages, lead to slower brain development? Or is there a mixture, depending on GA, and the presence of specific clinical predictors? These questions, and many of the limitations discussed above, can be tested using data from the developing Human Connectome Project (for example), which collected resting state fMRI data with $\sim$2,300 time-points and a TR of 0.39s. Additionally, they have many healthy term born controls as well.

Since completing this study, we have attempted the suggested follow-up investigation using data from the developing Human Connectome Project. The results from this new study [96] provides some initial answers to these questions.

Conclusions

To summarise, HE of the rs-fMRI BOLD signal was found to increase linearly from preterm to TEA in both grey matter and white matter, as well as in all RSNs. Evolving from more random

to a more ordered signal. HE in RSNs started around 0.67 at preterm age but increased significantly at different rates: from 0.76 in the frontal network to 0.84 in the motor network at TEA. This pattern appears to reflect previous findings that the general growth and maturation of RSNs occurs first and rapidly in sensory and motor networks, and associative networks such as frontal networks develop later on and more slowly. This is the first time this pattern has been shown by looking at the LRTC of low-sampled fMRI BOLD signal, an area of study that may provide greater insight into functional brain development.

Supporting information

S1 Fig. Group differences with and without term equivalent scans. Differences in gestational age (left), mean Framewise Displacement (centre) and post-menstrual age (right) were examined between subjects without term equivalent scans and those with. Gestational age was found to be higher in subjects with term equivalent scans, and was thus included in the mixed linear effects model.
(DOCX)

Acknowledgments

We would like to acknowledge and thank Dr Ziqi Sun for assistance and image acquisition.

Author Contributions

Conceptualization: Steven P. Miller, Ruth E. Grunau, Alexander M. Weber.

Data curation: Steven Ufkes.

Formal analysis: Johann P. Drayne, Allison E. Mella.

Funding acquisition: Steven P. Miller, Ruth E. Grunau, Alexander M. Weber.

Investigation: Alexander M. Weber.

Methodology: Mia M. McLean, Steven P. Miller, Ruth E. Grunau, Alexander M. Weber.

Project administration: Alexander M. Weber.

Resources: Vann Chau, Ting Guo, Helen M. Branson, Edmond Kelly, Alexander M. Weber.

Software: Johann P. Drayne, Alexander M. Weber.

Supervision: Alexander M. Weber.

Validation: Johann P. Drayne, Allison E. Mella, Steven P. Miller, Ruth E. Grunau, Alexander M. Weber.

Visualization: Johann P. Drayne, Alexander M. Weber.

Writing – original draft: Johann P. Drayne, Allison E. Mella, Mia M. McLean.

Writing – review & editing: Johann P. Drayne, Allison E. Mella, Steven P. Miller, Ruth E. Grunau, Alexander M. Weber.

References

1. Back SA, Miller SP. Brain Injury in Premature Neonates: A Primary Cerebral Dysmaturation Disorder? Annals of Neurology. 2014; 75(4):469–486. https://doi.org/10.1002/ana.24132 PMID: 24615937
2. Bonifacio SL, Glass HC, Chau V, Berman JI, Xu D, Brant R, et al. Extreme Premature Birth Is Not Associated with Impaired Development of Brain Microstructure. The Journal of Pediatrics. 2010; 157(5):726–732.e1. https://doi.org/10.1016/j.jpeds.2010.05.026 PMID: 20598316

3. Blencowe H, Lee AC, Cousens S, Bahalim A, Narwal R, Zhong N, et al. Preterm Birth–Associated Neurodevelopmental Impairment Estimates at Regional and Global Levels for 2010. Pediatric Research. 2013; 74(S1):17–34. https://doi.org/10.1038/pr.2013.204 PMID: 24366461

4. Chau V, Synnes A, Grunau RE, Poskitt KJ, Brant R, Miller SP. Abnormal Brain Maturation in Preterm Neonates Associated with Adverse Developmental Outcomes. Neurology. 2013; 81(24):2082–2089. https://doi.org/10.1212/01.wnl.0000437298.43688.b9 PMID: 24212394

5. Grunau RE. Neonatal Pain in Very Preterm Infants: Long-Term Effects on Brain, Neurodevelopment and Pain Reactivity. Rambam Maimonides Medical Journal. 2013; 4(4):e0025. https://doi.org/10.5041/RMMJ.10132 PMID: 24228168

6. Marlow N, Wolke D, Bracewell MA, Samara M, EPICure Study Group. Neurologic and Developmental Disability at Six Years of Age after Extremely Preterm Birth. The New England Journal of Medicine. 2005; 352(1):9–19. https://doi.org/10.1056/NEJMoa041367 PMID: 15635108

7. Schneider J, Duerden EG, Guo T, Ng K, Hagmann P, Bickle Graz M, et al. Procedural Pain and Oral Glucose in Preterm Neonates: Brain Development and Sex-Specific Effects. Pain. 2018; 159(3):515–525. https://doi.org/10.1097/j.pain.0000000000001123 PMID: 29200180

8. Ream MA, Lehwald L. Neurologic Consequences of Preterm Birth. Current Neurology and Neuroscience Reports. 2018; 18(8):48. https://doi.org/10.1007/s11910-018-0862-2 PMID: 29907917

9. Brenner RG, Wheelock MD, Neil JJ, Smyser CD. Structural and Functional Connectivity in Premature Neonates. Seminars in Perinatology. 2021; 45(7):151473. https://doi.org/10.1016/j.semperi.2021.151473 PMID: 34452753

10. Cho HJ, Jeong H, Park CA, Son DW, Shim SY. Altered Functional Connectivity in Children Born Very Preterm at School Age. Scientific Reports. 2022; 12(1):7308. https://doi.org/10.1038/s41598-022-11184-x PMID: 35508563

11. Smyser CD, Inder TE, Shimony JS, Hill JE, Degnan AJ, Snyder AZ, et al. Longitudinal Analysis of Neural Network Development in Preterm Infants. Cerebral Cortex. 2010; 20(12):2852–2862. https://doi.org/10.1093/cercor/bhq035 PMID: 20237243

12. Lee MH, Smyser CD, Shimony JS. Resting-State fMRI: A Review of Methods and Clinical Applications. American Journal of Neuroradiology. 2013; 34(10):1866–1872. https://doi.org/10.3174/ajnr.A3263 PMID: 22936095

13. Zimmern V. Why Brain Criticality Is Clinically Relevant: A Scoping Review. Frontiers in Neural Circuits. 2020; 14:54. https://doi.org/10.3389/fncir.2020.00054 PMID: 32982698

14. Maxim V, Sendur L, Fadili J, Suckling J, Gould R, Howard R, et al. Fractional Gaussian Noise, Functional MRI and Alzheimer's Disease. NeuroImage. 2005; 25(1):141–158. https://doi.org/10.1016/j.neuroimage.2004.10.044 PMID: 15734351

15. Sokunbi MO, Gradin VB, Waiter GD, Cameron GG, Ahearn TS, Murray AD, et al. Nonlinear Complexity Analysis of Brain fMRI Signals in Schizophrenia. PLoS ONE. 2014; 9(5):e95146. https://doi.org/10.1371/journal.pone.0095146 PMID: 24824731

16. Dona O, Hall GB, Noseworthy MD. Temporal Fractal Analysis of the Rs-BOLD Signal Identifies Brain Abnormalities in Autism Spectrum Disorder. PLOS ONE. 2017; 12(12):e0190081. https://doi.org/10.1371/journal.pone.0190081 PMID: 29272297

17. Lai MC, Lombardo MV, Chakrabarti B, Sadek SA, Pasco G, Wheelwright SJ, et al. A Shift to Randomness of Brain Oscillations in People with Autism. Biological Psychiatry. 2010; 68(12):1092–1099. https://doi.org/10.1016/j.biopsych.2010.06.027 PMID: 20728872

18. Weber AM, Soreni N, Noseworthy MD. A Preliminary Study on the Effects of Acute Ethanol Ingestion on Default Mode Network and Temporal Fractal Properties of the Brain. Magma (New York, NY). 2014; 27(4):291–301.

19. Dona O, Noseworthy MD, DeMatteo C, Connolly JF. Fractal Analysis of Brain Blood Oxygenation Level Dependent (BOLD) Signals from Children with Mild Traumatic Brain Injury (mTBI). PLOS ONE. 2017; 12(1):e0169647. https://doi.org/10.1371/journal.pone.0169647 PMID: 28072842

20. Campbell OL, Weber AM. Monofractal Analysis of Functional Magnetic Resonance Imaging: An Introductory Review. Human Brain Mapping. 2022; 43(8):2693–2706. https://doi.org/10.1002/hbm.25801 PMID: 35266236

21. Ciuciu P, Abry P, He BJ. Interplay between Functional Connectivity and Scale-Free Dynamics in Intrinsic fMRI Networks. NeuroImage. 2014; 95:248–263. https://doi.org/10.1016/j.neuroimage.2014.03.047 PMID: 24675649

22. He BJ. Scale-Free Properties of the Functional Magnetic Resonance Imaging Signal during Rest and Task. Journal of Neuroscience. 2011; 31(39):13786–13795. https://doi.org/10.1523/JNEUROSCI.2111-11.2011 PMID: 21957241

23. Buzsáki G, Mizuseki K. The Log-Dynamic Brain: How Skewed Distributions Affect Network Operations. Nature Reviews Neuroscience. 2014; 15(4):264–278. https://doi.org/10.1038/nrn3687 PMID: 24569488

24. Campbell O, Vanderwal T, Weber AM. Fractal-Based Analysis of fMRI BOLD Signal During Naturalistic Viewing Conditions. Frontiers in Physiology. 2021; 12:809943. https://doi.org/10.3389/fphys.2021.809943 PMID: 35087421

25. Churchill NW, Spring R, Grady C, Cimprich B, Askren MK, Reuter-Lorenz PA, et al. The Suppression of Scale-Free fMRI Brain Dynamics across Three Different Sources of Effort: Aging, Task Novelty and Task Difficulty. Scientific Reports. 2016; 6(1):30895. https://doi.org/10.1038/srep30895 PMID: 27498696

26. Barnes A, Bullmore ET, Suckling J. Endogenous Human Brain Dynamics Recover Slowly Following Cognitive Effort. PLoS ONE. 2009; 4(8):e6626. https://doi.org/10.1371/journal.pone.0006626 PMID: 19680553

27. Padilla N, Saenger VM, van Hartevelt TJ, Fernandes HM, Lennartsson F, Andersson JLR, et al. Breakdown of Whole-brain Dynamics in Preterm-born Children. Cerebral Cortex. 2020; 30(3):1159–1170. https://doi.org/10.1093/cercor/bhz156 PMID: 31504269

28. Hartley C, Berthouze L, Mathieson SR, Boylan GB, Rennie JM, Marlow N, et al. Long-Range Temporal Correlations in the EEG Bursts of Human Preterm Babies. PLoS ONE. 2012; 7(2):e31543. https://doi.org/10.1371/journal.pone.0031543 PMID: 22363669

29. Li X, Morgan PS, Ashburner J, Smith J, Rorden C. The First Step for Neuroimaging Data Analysis: DICOM to NIfTI Conversion. Journal of Neuroscience Methods. 2016; 264:47–56. https://doi.org/10.1016/j.jneumeth.2016.03.001 PMID: 26945974

30. Tustison NJ, Avants BB, Cook PA, Zheng Y, Egan A, Yushkevich PA, et al. N4ITK: Improved N3 Bias Correction. IEEE transactions on medical imaging. 2010; 29(6):1310–1320. https://doi.org/10.1109/TMI.2010.2046908 PMID: 20378467

31. Tustison NJ, Cook PA, Klein A, Song G, Das SR, Duda JT, et al. Large-Scale Evaluation of ANTs and FreeSurfer Cortical Thickness Measurements. NeuroImage. 2014; 99:166–179. https://doi.org/10.1016/j.neuroimage.2014.05.044 PMID: 24879923

32. Makropoulos A, Robinson EC, Schuh A, Wright R, Fitzgibbon S, Bozek J, et al. The Developing Human Connectome Project: A Minimal Processing Pipeline for Neonatal Cortical Surface Reconstruction. NeuroImage. 2018; 173:88–112. https://doi.org/10.1101/125526 PMID: 29409960

33. Smith SM. Fast Robust Automated Brain Extraction. Human Brain Mapping. 2002; 17(3):143–155. https://doi.org/10.1002/hbm.10062 PMID: 12391568

34. Makropoulos A, Gousias IS, Ledig C, Aljabar P, Serag A, Hajnal JV, et al. Automatic Whole Brain MRI Segmentation of the Developing Neonatal Brain. IEEE Transactions on Medical Imaging. 2014; 33(9):1818–1831. https://doi.org/10.1109/TMI.2014.2322280 PMID: 24816548

35. Jenkinson M, Bannister P, Brady M, Smith S. Improved Optimization for the Robust and Accurate Linear Registration and Motion Correction of Brain Images. NeuroImage. 2002; 17(2):825–841. https://doi.org/10.1006/nimg.2002.1132 PMID: 12377157

36. Power JD, Barnes KA, Snyder AZ, Schlaggar BL, Petersen SE. Spurious but Systematic Correlations in Functional Connectivity MRI Networks Arise from Subject Motion. NeuroImage. 2012; 59(3):2142–2154. https://doi.org/10.1016/j.neuroimage.2011.10.018 PMID: 22019881

37. Fitzgibbon SP, Harrison SJ, Jenkinson M, Baxter L, Robinson EC, Bastiani M, et al. The Developing Human Connectome Project (dHCP) Automated Resting-State Functional Processing Framework for Newborn Infants. NeuroImage. 2020; 223:117303. https://doi.org/10.1016/j.neuroimage.2020.117303 PMID: 32866666

38. Salimi-Khorshidi G, Douaud G, Beckmann CF, Glasser MF, Griffanti L, Smith SM. Automatic Denoising of Functional MRI Data: Combining Independent Component Analysis and Hierarchical Fusion of Classifiers. NeuroImage. 2014; 90:449–468. https://doi.org/10.1016/j.neuroimage.2013.11.046 PMID: 24389422

39. Griffanti L, Salimi-Khorshidi G, Beckmann CF, Auerbach EJ, Douaud G, Sexton CE, et al. ICA-based Artefact Removal and Accelerated fMRI Acquisition for Improved Resting State Network Imaging. NeuroImage. 2014; 95:232–247. https://doi.org/10.1016/j.neuroimage.2014.03.034 PMID: 24657355

40. Griffanti L, Douaud G, Bijsterbosch J, Evangelisti S, Alfaro-Almagro F, Glasser MF, et al. Hand Classification of fMRI ICA Noise Components. NeuroImage. 2017; 154:188–205. https://doi.org/10.1016/j.neuroimage.2016.12.036 PMID: 27989777

41. Kelly RE, Alexopoulos GS, Wang Z, Gunning FM, Murphy CF, Morimoto SS, et al. Visual Inspection of Independent Components: Defining a Procedure for Artifact Removal from fMRI Data. Journal of Neuroscience Methods. 2010; 189(2):233–245. https://doi.org/10.1016/j.jneumeth.2010.03.028 PMID: 20381530

42. Smith SM, Brady JM. SUSAN—A New Approach to Low Level Image Processing. International Journal of Computer Vision. 1997; 23(1):45–78. https://doi.org/10.1023/A:1007963824710

43. Beckmann CF, Smith SM. Probabilistic Independent Component Analysis for Functional Magnetic Resonance Imaging. IEEE transactions on medical imaging. 2004; 23(2):137–152. https://doi.org/10.1109/TMI.2003.822821 PMID: 14964560

44. Doria V, Beckmann CF, Arichi T, Merchant N, Groppo M, Turkheimer FE, et al. Emergence of Resting State Networks in the Preterm Human Brain. Proceedings of the National Academy of Sciences. 2010; 107(46):20015–20020. https://doi.org/10.1073/pnas.1007921107 PMID: 21041625

45. Eke A, Hermán P, Bassingthwaighte J, Raymond G, Percival D, Cannon M, et al. Physiological Time Series: Distinguishing Fractal Noises from Motions. Pflügers Archiv—European Journal of Physiology. 2000; 439(4):403–415. https://doi.org/10.1007/s004249900135 PMID: 10678736

46. Bullmore E, Fadili J, Maxim V, Şendur L, Whitcher B, Suckling J, et al. Wavelets and Functional Magnetic Resonance Imaging of the Human Brain. NeuroImage. 2004; 23:S234–S249. https://doi.org/10.1016/j.neuroimage.2004.07.012 PMID: 15501094

47. Welch P. The Use of Fast Fourier Transform for the Estimation of Power Spectra: A Method Based on Time Averaging over Short, Modified Periodograms. IEEE Transactions on Audio and Electroacoustics. 1967; 15(2):70–73. https://doi.org/10.1109/TAU.1967.1161901

48. Virtanen P, Gommers R, Oliphant TE, Haberland M, Reddy T, Cournapeau D, et al. SciPy 1.0: Fundamental Algorithms for Scientific Computing in Python. Nature Methods. 2020; 17(3):261–272. https://doi.org/10.1038/s41592-019-0686-2 PMID: 32015543

49. Rubin D, Fekete T, Mujica-Parodi LR. Optimizing Complexity Measures for fMRI Data: Algorithm, Artifact, and Sensitivity. PLoS ONE. 2013; 8(5):e63448. https://doi.org/10.1371/journal.pone.0063448 PMID: 23700424

50. R Core Team. R: A Language and Environment for Statistical Computing; 2022. R Foundation for Statistical Computing.

51. RStudio Team. RStudio: Integrated Development Environment for R;. RStudio, PBC.

52. Bates D, Mächler M, Bolker B, Walker S. Fitting Linear Mixed-Effects Models Using **Lme4**. Journal of Statistical Software. 2015; 67(1). https://doi.org/10.18637/jss.v067.i01

53. Russell V Lenth. Emmeans: Estimated Marginal Means, Aka Least-Squares Means; 2022.

54. Bullmore ET, Brammer MJ, Bourlon P, Alarcon G, Polkey CE, Elwes R, et al. Fractal Analysis of Electroencephalographic Signals Intracerebrally Recorded during 35 Epileptic Seizures: Evaluation of a New Method for Synoptic Visualisation of Ictal Events. Electroencephalography and Clinical Neurophysiology. 1994; 91(5):337–345. https://doi.org/10.1016/0013-4694(94)00181-2 PMID: 7525230

55. Wink AM, Bullmore E, Barnes A, Bernard F, Suckling J. Monofractal and Multifractal Dynamics of Low Frequency Endogenous Brain Oscillations in Functional MRI. Human Brain Mapping. 2008; 29(7):791–801. https://doi.org/10.1002/hbm.20593 PMID: 18465788

56. Bullmore E, Long C, Suckling J, Fadili J, Calvert G, Zelaya F, et al. Colored Noise and Computational Inference in Neurophysiological (fMRI) Time Series Analysis: Resampling Methods in Time and Wavelet Domains. Human Brain Mapping. 2001; 12(2):61–78. https://doi.org/10.1002/1097-0193(200102)12:2<61::AID-HBM1004>3.0.CO;2-W PMID: 11169871

57. He BJ, Zempel JM, Snyder AZ, Raichle ME. The Temporal Structures and Functional Significance of Scale-free Brain Activity. Neuron. 2010; 66(3):353–369. https://doi.org/10.1016/j.neuron.2010.04.020 PMID: 20471349

58. Omidvarnia A, Zalesky A, Mansour L S, Van De Ville D, Jackson GD, Pedersen M. Temporal Complexity of fMRI Is Reproducible and Correlates with Higher Order Cognition. NeuroImage. 2021; 230:117760. https://doi.org/10.1016/j.neuroimage.2021.117760 PMID: 33486124

59. Caserta F, Eldred WD, Fernandez E, Hausman RE, Stanford LR, Bulderev SV, et al. Determination of Fractal Dimension of Physiologically Characterized Neurons in Two and Three Dimensions. Journal of Neuroscience Methods. 1995; 56(2):133–144. https://doi.org/10.1016/0165-0270(94)00115-W PMID: 7752679

60. Lowen SB, Cash SS, Poo M, Teich MC. Quantal Neurotransmitter Secretion Rate Exhibits Fractal Behavior. The Journal of Neuroscience: The Official Journal of the Society for Neuroscience. 1997; 17(15):5666–5677. https://doi.org/10.1523/JNEUROSCI.17-15-05666.1997 PMID: 9221766

61. Mazzoni A, Broccard FD, Garcia-Perez E, Bonifazi P, Ruaro ME, Torre V. On the Dynamics of the Spontaneous Activity in Neuronal Networks. PLoS ONE. 2007; 2(5):e439. https://doi.org/10.1371/journal.pone.0000439 PMID: 17502919

62. Bédard C, Destexhe A. Macroscopic Models of Local Field Potentials and the Apparent 1/f Noise in Brain Activity. Biophysical Journal. 2009; 96(7):2589–2603. https://doi.org/10.1016/j.bpj.2008.12.3951 PMID: 19348744

63. Kitzbichler MG, Smith ML, Christensen S, Bullmore ET. Broadband Criticality of Human Brain Network Synchronization. PLOS Computational Biology. 2009; 5(3):1–13. https://doi.org/10.1371/journal.pcbi.1000314 PMID: 19300473

64. Tagliazucchi E, Balenzuela P, Fraiman D, Chialvo DR. Criticality in Large-Scale Brain FMRI Dynamics Unveiled by a Novel Point Process Analysis. Frontiers in Physiology. 2012; 3:15–15. https://doi.org/10.3389/fphys.2012.00015 PMID: 22347863

65. Beggs JM. The Criticality Hypothesis: How Local Cortical Networks Might Optimize Information Processing. Philosophical Transactions of the Royal Society A: Mathematical, Physical and Engineering Sciences. 2008; 366(1864):329–343. https://doi.org/10.1098/rsta.2007.2092 PMID: 17673410

66. Shew WL, Plenz D. The Functional Benefits of Criticality in the Cortex. The Neuroscientist. 2013; 19 (1):88–100. https://doi.org/10.1177/1073858412445487 PMID: 22627091

67. Maass W, Natschläger T, Markram H. Real-Time Computing Without Stable States: A New Framework for Neural Computation Based on Perturbations. Neural Computation. 2002; 14(11):2531–2560. https://doi.org/10.1162/089976602760407955 PMID: 12433288

68. Bertschinger N, Natschläger T. Real-Time Computation at the Edge of Chaos in Recurrent Neural Networks. Neural Computation. 2004; 16(7):1413–1436. https://doi.org/10.1162/089976604323057443 PMID: 15165396

69. Nirenberg S, Latham PE. Decoding Neuronal Spike Trains: How Important Are Correlations? Proceedings of the National Academy of Sciences. 2003; 100(12):7348–7353. https://doi.org/10.1073/pnas.1131895100 PMID: 12775756

70. Haldeman C, Beggs JM. Critical Branching Captures Activity in Living Neural Networks and Maximizes the Number of Metastable States. Physical Review Letters. 2005; 94(5):058101. https://doi.org/10.1103/PhysRevLett.94.058101 PMID: 15783702

71. Kinouchi O, Copelli M. Optimal Dynamical Range of Excitable Networks at Criticality. Nature Physics. 2006; 2(5):348–351. https://doi.org/10.1038/nphys289

72. Tanaka S, Miyashita M. Constraint on the Number of Synaptic Inputs to a Visual Cortical Neuron Controls Receptive Field Formation. Neural Computation. 2009; 21(9):2554–2580. https://doi.org/10.1162/neco.2009.04-08-752 PMID: 19548800

73. Grajauskas LA, Frizzell T, Song X, D'Arcy RCN. White Matter fMRI Activation Cannot Be Treated as a Nuisance Regressor: Overcoming a Historical Blind Spot. Frontiers in Neuroscience. 2019; 13:1024. https://doi.org/10.3389/fnins.2019.01024 PMID: 31636527

74. Bianciardi M, Fukunaga M, van Gelderen P, de Zwart JA, Duyn JH. Negative BOLD-fMRI Signals in Large Cerebral Veins. Journal of Cerebral Blood Flow and Metabolism: Official Journal of the International Society of Cerebral Blood Flow and Metabolism. 2011; 31(2):401–412. https://doi.org/10.1038/jcbfm.2010.164 PMID: 20859295

75. Liu CY, Krishnan AP, Yan L, Smith RX, Kilroy E, Alger JR, et al. Complexity and Synchronicity of Resting State Blood Oxygenation Level-Dependent (BOLD) Functional MRI in Normal Aging and Cognitive Decline. Journal of magnetic resonance imaging: JMRI. 2013; 38(1):36–45. https://doi.org/10.1002/jmri.23961 PMID: 23225622

76. Dong J, Jing B, Ma X, Liu H, Mo X, Li H. Hurst Exponent Analysis of Resting-State fMRI Signal Complexity across the Adult Lifespan. Frontiers in Neuroscience. 2018; 12:34. https://doi.org/10.3389/fnins.2018.00034 PMID: 29456489

77. Kostović I, Jovanov-Milošević N. The Development of Cerebral Connections during the First 20–45 Weeks' Gestation. Seminars in Fetal and Neonatal Medicine. 2006; 11(6):415–422. https://doi.org/10.1016/j.siny.2006.07.001 PMID: 16962836

78. Fransson P, Metsäranta M, Blennow M, Åden U, Lagercrantz H, Vanhatalo S. Early Development of Spatial Patterns of Power-Law Frequency Scaling in fMRI Resting-State and EEG Data in the Newborn Brain. Cerebral Cortex. 2013; 23(3):638–646. https://doi.org/10.1093/cercor/bhs047 PMID: 22402348

79. Cao M, He Y, Dai Z, Liao X, Jeon T, Ouyang M, et al. Early Development of Functional Network Segregation Revealed by Connectomic Analysis of the Preterm Human Brain. Cerebral Cortex. 2016; p. bhw038. https://doi.org/10.1093/cercor/bhw038

80. Fransson P, Skiöld B, Horsch S, Nordell A, Blennow M, Lagercrantz H, et al. Resting-State Networks in the Infant Brain. Proceedings of the National Academy of Sciences. 2007; 104(39):15531–15536. https://doi.org/10.1073/pnas.0704380104 PMID: 17878310

81. Fransson P, Skiöld B, Engström M, Hallberg B, Mosskin M, Åden U, et al. Spontaneous Brain Activity in the Newborn Brain During Natural Sleep—An fMRI Study in Infants Born at Full Term. Pediatric Research. 2009; 66(3):301–305. https://doi.org/10.1203/PDR.0b013e3181b1bd84 PMID: 19531974

82. Gao W, Lin W, Grewen K, Gilmore JH. Functional Connectivity of the Infant Human Brain: Plastic and Modifiable. The Neuroscientist. 2017; 23(2):169–184. https://doi.org/10.1177/1073858416635986 PMID: 26929236

83. Gao W, Alcauter S, Elton A, Hernandez-Castillo CR, Smith JK, Ramirez J, et al. Functional Network Development During the First Year: Relative Sequence and Socioeconomic Correlations. Cerebral Cortex. 2015; 25(9):2919–2928. https://doi.org/10.1093/cercor/bhu088 PMID: 24812084

84. Colonnese M, Khazipov R. Spontaneous Activity in Developing Sensory Circuits: Implications for Resting State fMRI. NeuroImage. 2012; 62(4):2212–2221. https://doi.org/10.1016/j.neuroimage.2012.02.046 PMID: 22387472

85. Dubois J, Dehaene-Lambertz G, Kulikova S, Poupon C, Hüppi PS, Hertz-Pannier L. The Early Development of Brain White Matter: A Review of Imaging Studies in Fetuses, Newborns and Infants. Neuroscience. 2014; 276:48–71. https://doi.org/10.1016/j.neuroscience.2013.12.044 PMID: 24378955

86. Hagmann P, Sporns O, Madan N, Cammoun L, Pienaar R, Wedeen VJ, et al. White Matter Maturation Reshapes Structural Connectivity in the Late Developing Human Brain. Proceedings of the National Academy of Sciences. 2010; 107(44):19067–19072. https://doi.org/10.1073/pnas.1009073107 PMID: 20956328

87. Weber AM, Zhang Y, Kames C, Rauscher A. Myelin Water Imaging and R_2 * Mapping in Neonates: Investigating R_2 * Dependence on Myelin and Fibre Orientation in Whole Brain White Matter. NMR in Biomedicine. 2020; 33(3). https://doi.org/10.1002/nbm.4222 PMID: 31846134

88. Deoni SCL, Mercure E, Blasi A, Gasston D, Thomson A, Johnson M, et al. Mapping Infant Brain Myelination with Magnetic Resonance Imaging. The Journal of Neuroscience: The Official Journal of the Society for Neuroscience. 2011; 31(2):784–791. https://doi.org/10.1523/JNEUROSCI.2106-10.2011 PMID: 21228187

89. Sugihara G, May R, Ye H, Hsieh Ch, Deyle E, Fogarty M, et al. Detecting Causality in Complex Ecosystems. Science. 2012; 338(6106):496–500. https://doi.org/10.1126/science.1227079 PMID: 22997134

90. Li J, Convertino M. Inferring Ecosystem Networks as Information Flows. Scientific Reports. 2021; 11 (1):7094. https://doi.org/10.1038/s41598-021-86476-9 PMID: 33782461

91. Motlaghian SM, Belger A, Bustillo JR, Ford JM, Iraji A, Lim K, et al. Nonlinear Functional Network Connectivity in Resting Functional Magnetic Resonance Imaging Data. Human Brain Mapping. 2022; 43 (15):4556–4566. https://doi.org/10.1002/hbm.25972 PMID: 35762454

92. Gourévitch B, Bouquin-Jeannès RL, Faucon G. Linear and Nonlinear Causality between Signals: Methods, Examples and Neurophysiological Applications. Biological Cybernetics. 2006; 95(4):349–369. https://doi.org/10.1007/s00422-006-0098-0 PMID: 16927098

93. Pianosi F, Beven K, Freer J, Hall JW, Rougier J, Stephenson DB, et al. Sensitivity Analysis of Environmental Models: A Systematic Review with Practical Workflow. Environmental Modelling & Software. 2016; 79:214–232. https://doi.org/10.1016/j.envsoft.2016.02.008

94. flax. Global Sensitivity Analysis Toolbox; 2024. https://www.mathworks.com/matlabcentral/fileexchange/40759-global-sensitivity-analysis-toolbox.

95. Chrostowski R, Li Z, Smith J, Mangolini F. Monte-Carlo Evaluation of Bias and Variance in Hurst Exponents Computed from Power Spectral Analysis of Atomic Force Microscopy Topographic Images. Applied Surface Science. 2022; 581:152092. https://doi.org/10.1016/j.apsusc.2021.152092

96. Mella AE, Vanderwal Tamara, Miller Steven P, Weber Alexander M. Temporal Complexity of the BOLD-Signal In Preterm Versus Term Infants. Cerebral Cortex. 2024; 34(11). https://doi.org/10.1093/cercor/bhae426